Preprint Title	Two-step single-reactor synthesis of oleic acid- or undecylenic acid-stabilized magnetic nanoparticles by thermal decomposition method
Authors	Mykhailo Nahorniak, Pamela Pasetto, Jean-Marc Greneche, Volodymyr Samaryk, Sandy Auguste, Anthony Rousseau, Nataliya Nosova and Serhii Varvarenko
Publication Date	02 März 2022
Article Type	Full Research Paper
ORCID® iDs	Mykhailo Nahorniak - https://orcid.org/0000-0003-2586-9741; Sandy Auguste - https://orcid.org/0000-0002-3777-9527; Anthony Rousseau - https://orcid.org/0000-0002-5074-824X

wo-step single-reactor synthesis of oleic acid- or undecylenic acid-stabilized magnetic nanoparticles by thermal decomposition method

Mykhailo Nahorniak[1,3], Pamela Pasetto[2], Jean-Marc Greneche[2], Volodymyr Samaryk[1], Sandy Auguste[2], Anthony Rousseau[2], Nataliya Nosova[1], Serhii Varvarenko*[1]

[1]Organic Chemistry department, Lviv Polytechnic National University, Bandera street 12, 79013, Lviv, Ukraine

[2]Institut des Molécules et Matériaux du Mans (IMMM), UMR 6283 CNRS − Le Mans Université, Avenue Olivier Messiaen, 72085 Le Mans Cedex, France

[3]Polymeric particles department, Institute of Macromolecular Chemistry CAS, Heyrovského nám. 2, 162 06 Prague 6, Czech Republic

Corresponding author: Serhii Varvarenko, serhii.m.varvarenko@lpnu.ua

Abstract

Different iron oxides (i.e., magnetite, maghemite, goethite, wüstite) show distinct effects on biological objects, and thus the investigations of the morphology and phase-structural state have prime priority for their biomedical applications.

The aim of this work was to develop one-pot synthesis of magnetic nanoparticles by thermolysis of Fe(III)-oleate or Fe(III)-undecylate in a high-boiling point solvent *in situ*, using Fe(III)-acetylacetonate. Magnetic nanoparticles were characterized by transmission electron microscopy, dynamic light scattering, thermogravimetric analysis, ATR-FTIR and 57Fe Mössbauer spectroscopy, X-ray diffraction in terms of morphology, hydrodynamic diameter and composition, respectively. The effect of the solvent and unsaturated higher carboxylic acid, used as a reagent and nanoparticles stabilizer, on the particles' properties was investigated. Synthesis using undecylenic acid led to the formation of iron oxide particles with larger diameter

(11-16 nm according to TEM) which were in 75% formed of magnetite. According to the Mössbauer and XRD results, the organic shell thickness around the nanoparticles depended on the nature of the stabilizer, but it did not prevent the partial oxidation of the particles magnetite core to maghemite. In contrast, monodisperse single-domain maghemite nanoparticles with size less than 8 nm were synthesized using oleic acid in 1-octadecene.

Keywords

Iron oxide nanoparticles, Fe(III)-acetylacetonate, thermal decomposition synthesis, maghemite, magnetite

Introduction

Magnetic nanoparticles are increasingly used in various fields thanks to the recent progress in their controlled synthesis and knowledge of their chemical and physical properties. One of such areas is biomedicine[1]. Especially, iron oxide-based nanoparticles, due to their biodegradation, low toxicity, and enhanced oxidative resistance compared to metallic nanoparticles show high potential in biomedical applications[2,3,4]. Up to now, iron oxide nanoparticles were proposed as contrast agents for magnetic resonance imaging, high-precision biosensors, as well as carriers in magnetic-assisted drug delivery systems. Furthermore, they have been applied for tumour treatment using hyperthermia method[5] and in bone tissue regenerative medicine[6].

However, the use of iron oxide nanoparticles in biomedicine firstly requires in-depth studies of their structure and properties. It was well-established that different iron oxides, e.g., magnetite (Fe_3O_4), maghemite (γ-Fe_2O_3), goethite (α-FeOOH), and wüstite (FeO), have divergent impact on biological objects[7]. In this regard, the study of the morphology and phase composition of iron oxide-based nanoparticles is critical issue. Nevertheless, magnetite and maghemite particles remain the most commonly used nanoparticles in biomedical applications. However, it has to be noted that magnetite nanoparticles undergo rapid oxidation in air, which leads to the formation of the maghemite layer on their surface. The oxidation is significantly

enhanced in case of nanoparticles characterized by large specific surface area, and thus it can be concluded that the smaller the nanoparticles are, the higher the maghemite content is. In addition, micro- and nanosized particles differ significantly in their magnetic properties[8]. Microsized nanoparticles are typically multi-domain and ferrimagnetic, while nanoparticles below 20-30 nm are usually single-domain. Further reduction of the nanoparticles diameter below the critical size leads to the obtaining of nanoparticles with superparamagnetic properties[9,10]. Thanks to the absence of coercive forces in superparamagnetic nanoparticles not exposed upon external magnetic field, they are characterized by good colloidal stability, which make them ideal candidates, e.g., for magnetic-assisted targeted drug delivery[11].

Nanoscale magnetite can be obtained by various well-known synthesis routes, such as hydrothermal synthesis, thermal decomposition or coprecipitation method[9,10]. Each of these synthetic approaches has certain advantages and disadvantages. One of the essential issues in many biomedical applications is synthesis of magnetic nanoparticles with uniform size and chemical composition, and superparamagnetic properties. These requirements can be meet by applying the thermal decomposition method, which is based on the decay of low-stable organic iron salts (i.e, acetate, pentacarbonyl, acetylacetonate) in a high boiling point solvents, in the presence of stabilizing agents, e.g., fatty acids, higher amines, alcohols, or their mixtures[12,13,20]. Although thermal decomposition method is relatively simple, there is no single way for its implementation; changing the reaction time and conditions considerably influences the properties of the final nanoparticles. Apart from the narrow size distribution of the particles, the possibility of preparing particles of various morphology (e.g., spherical, cubic, octahedral) is a next great advantage of this method over the coprecipitation one[14,15].

Previously, the decomposition of thermally unstable Fe(III)-acetylacetonate at temperature above 150 °C, directly leading to the formation of iron oxide nanoparticles when an oleylamine was used as a stabilizer, have been reported[16]. In these conditions, FeO/Fe_3O_4 nanoparticles were obtained[17]. To synthesise magnetite nanoparticles, an additional component, e.g., 1,2-hexadecandiol, was introduced into the system[18]. Optionally, if Fe(III)-

oleate was pre-synthesized the magnetite nanoparticles were the product of thermolysis in high-boiling point solvent (at 250-320 °C)[19]. Up to date, there is no publications about the two- step single-reactor synthesis of iron oxide magnetic nanoparticles by thermal decomposition method, in which Fe(III)-acetylacetonate is used as starting compound for the synthesis of alkanoates followed by thermolysis of their solution.

The aim of this work was first to develop the synthesis of nanomagnetite dispersions by thermolysis of Fe(III)-oleate or Fe(III)-undecylate in a high-boiling point solvent *in situ* using Fe(III)-acetylacetonate as the precursor, and then to study the structure and morphology of the obtained nanoparticles using various complementary characterization techniques.

Results and Discussion

The physicochemical properties of magnetite nanoparticles synthesized via the thermal decomposition method depend on many factors, such as selection of precursor and organic stabilizer, ligand/precursor ratio, solvent, and temperature of the decomposition reaction. In this study, a series of dispersions of magnetic nanoparticles were obtained using various solvents and stabilizing agents (Table 1). All prepared nanoparticles were initially black[20] but slowly became reddish upon exposure to air. When the synthesis was carried out at a slight excess of fatty acids, the unstable dispersions of particles were obtained, which coagulated and formed a black magnetic precipitate on the reactor walls (TM-III; precursor/fatty acid molar ratio of 1:3.05). Applying molar ratio of Fe(III)-acetylacetonate to carboxylic acid of 1:3.29 resulted in partially stable dispersions of the nanoparticles (TM-I, TM-VI). In contrast, a brown liquid, containing neither particles nor magnetic sediment, was obtained when a large excess of stabilizing agent (above molar ratio of 1:5.5) was used.

Although there are number of publications, which explain the processes of the formation of magnetic nanoparticles during the thermal decomposition, it is noteworthy to examine applied in this study system in more detail. In the presence of higher carboxylic acid, such as oleic acid (OA) or undecylenic acid (UA, Fe(III)-alkanoate is a predominant product of Fe(III)-

acetylacetonate decomposition at relatively low-temperature range of 110-120 °C (Figure 1). To avoid the influence of acetylacetone residues, which are formed during the decomposition of acetylacetonate, they were removed from the reaction mixture under vacuum. Consequently, the reaction mixture contained only Fe(III)-alkanoate in an appropriate solvent and a set amount of higher fatty acid.

Thermal decomposition of Fe(III)-alkanoate at temperatures below 200 °C occurs at a negligible rate, and thus its impact is insignificant[21]. Above 200 °C, i.e. 310-312 °C in case of 1-octadecene and at 255 °C for diphenyl and paraffin, Fe(III)-alkanoate undergoes decarboxylation thermolysis accompanied by breaking of FeO-C bonds. The release of carbon mono- and dioxide, hydrogen, higher ketones, and hydrocarbons, as well as partial reduction of Fe(III) to Fe(II), result in a formation of magnetic iron oxide nanoparticles[22]. Excess of higher carboxylic acid that has not been bound to the iron salt did not undergo to thermolysis and is likely to being adsorbed on the surface of the particles ensuring the stability of the nanodispersion (Figure 2)[23].

TEM microphotographs of the prepared nanoparticles confirmed their size between 8 and 16 nm (Figure 3, 4). The diameter and shape of the nanoparticles depended on the preparation conditions, especially selection of the higher fatty acid – the OA-stabilized nanoparticles were significantly smaller (8-13 nm) compare to UA-stabilized ones (11-16 nm). Furthermore, the highly monodispersed spherical nanoparticles, creating the stable dispersions toluene, were obtained only when 1-octadecene was used as a solvent (Figure 3, Table 1). The majority of the nanoparticles synthesised in paraffin and diphenyl were poorly reproducible and non-uniform in size and shape. Only the MT-IV nanoparticles, which were synthesised at twice as low concentration of the reagents in paraffin compared to the rest of the synthetic approaches, were spherical (Figure 4). However, the yield of this synthesis was significantly lower compared to ones conducted in 1-octadecene. The Miller indexes on the electron diffraction patterns (Figure 5) of the radiating crystallographic planes were presented as SAED patterns and corresponded clearly to a spinel phase, typical for both magnetite and maghemite. Moreover, the fact that the

halos observed were uniform and the single spots were not visible proved that the crystallites were very small. These results corresponded well with data achieved from XRD diffraction, according to which the average size of the crystallites for all prepared nanoparticles was in the range of 4.5-9 nm. The average crystallite size did not correlate with the amount of stabilizer used. The Rietveld refinement allowed to determine a coherent diffracting domain size nanoparticle of 6 nm by using LaB_6 as a reference compound (Table 1). The particularly good agreement of indices (R_{exp}=0.44, R_p=1.17, R_{wp}=1.75, R_{Bragg}=24.23 and GoF=15.55) confirmed a proper refinement. The size determined from the TEM microphotographs of the particles synthesized using OA (8-13 nm) was generally closer to the average size of the crystallites obtained by estimating the expansion of the X-ray diffraction line (D_{XRD} calculated with Scherer, optionally Rietveld, refinement), which indicated a single magnetic domain character of the TMO-I nanoparticles. Using a stabilizer with shorter carbon chain, i.e., UA, under the same synthetic conditions resulted in particles of larger size (11-16 nm). These particles were characterized by a significantly higher polycrystalline index (I_{PCR} = 2.5- 3.5) and were likely aggregates of the crystallites of smaller size, which also corelated with higher polydispersity index observed for these nanoparticles (Table 1).

The X-ray diffraction patterns of the synthesised nanoparticles were compared to standard ones both of magnetite and maghemite (Figure 6). The diffraction patterns of the synthesised nanoparticles showed the great similarity to the patterns of the standards. However, it has to be noted that both these iron oxides are characterized by spinal-structures and very close lattice parameters, which makes their distinction using XRD very troublesome[24].

In contrast to XRD, ^{57}Fe Mössbauer spectrometry allows to discriminate magnetite and maghemite as the isomer shift, resulting from the monopolar electric interactions, is very sensitive to the Fe valency states. Considering the characteristic measurement time of ^{57}Fe Mössbauer spectrometry estimated at 10^{-8} s from the Larmor frequency, the hyperfine structure of magnetite at 300 K (and above the Verwey transition estimated at 119 K) is composed of one-third of Fe^{3+} species and two-thirds of $Fe^{2.5+}$ species in accordance with its expected

electronic and stoichiometric structure. The Mössbauer spectra of the TMO-I nanoparticles at 300 K and 77 K were shown in Figure 7. At 300 K, a broadened single line typical for the presence of superparamagnetic relaxation phenomena suggesting a very small size (about 10 nm compared to results from literature) of the synthesised nanoparticles, which was consistent with the electron and XRD diffraction results, as well as TEM results. Different fitting models can be considered using either a distribution of hyperfine fields or a superimposition of two single lines giving rise to an invariant mean value of isomer shift consistent with the presence of only Fe^{3+} species. In contrast, the Mössbauer spectrum recorded at 77 K consisted of a pure symmetrical magnetic sextet composed of broadened and asymmetrical lines that can be well described by using a discrete distribution of hyperfine fields, also giving rise to a mean value of isomer shift consistent with the presence of only Fe^{3+} species. Thus, it can be concluded that these nanoparticles are monodispersed and exclusively made up of maghemite. According to previous studies reported in the literature, magnetite-maghemite core-shell nanoparticles can by prepared by partial oxidation of magnetite core during and/or after synthesis and the thickness of its shell can be controlled. Furthermore, the prolonger oxidation may result to production of maghemite nanoparticles. These observations are in agreement with the result of the present study, confirming the monodisperse nature of the maghemite nanoparticles obtained.

The TMY-5 nanoparticles were also measured at 300 K and 77 K (Figure 7). The profiles differed from those observed on TMO-I; the shape of the single line at 300 K and the better-defined hyperfine structure at 77 K indicated a decrease in superparamagnetic relaxation phenomena, likely caused by bigger size of the nanoparticles. In addition, the spectrum collected at 77 K can be decomposed into four different components: *(i)* three magnetic ones are attributed to blocked Fe^{3+} species, blocked Fe^{2+} species, and Fe ions having intermediate valency states between Fe^{3+} and Fe^{2+}, as usually observed in typical magnetite below the Verwey transition and *(ii)* a quadrupolar component assigned to Fe^{2+} species, probably some traces (4%) of FeO (wüstite). However, the values of hyperfine parameters, particularly the mean values of isomer shift (independent of the fitting model), indicated the mixed phase

composition of the nanoparticles, i.e., maghemite: magnetite in ratio of 25:75 in terms of Fe atomic proportions, thus proving their partial oxidation[25,26].

The ATR-FTIR and TGA were used to for surface characterization in terms of the presence of higher fatty acid, which play important role for the particle's stability and future functionality. ATR FTIR studies confirmed the presence of characteristic bands that could be assigned to the organic (stabilizing) layer on the surface of nanoparticles synthesized with both OA (TMO-I) and UA (TMY-II) (Figure 5). The peaks at 2850 and 2920 cm^{-1} were attributed to symmetric and asymmetric stretching vibrations of CH_2 groups of carboxylic acid. The band at 1710 cm^{-1} corresponded to vibrations of the C=O group, not involved in hydrogen bonds[27]. The peaks at 1640, 1456, and 1377 cm^{-1} were ascribed to the deformation fluctuations in isolated double C=C bonds in OA and UA, whereas the bands at 1560 and 1430 cm^{-1} corresponded to symmetric and asymmetric vibrations of COO^- groups of the stabilizing layer, attached to the core of the nanoparticles. The intense peak at 582 cm^{-1} was attributed to oscillation of the Fe-O.

The thickness of organic shell was estimated by comparing the hydrodynamic diameter of the particle with its size determined from TEM microphotographs (Table 1). For the UA-stabilized nanoparticles, the thickness of organic layer was of 8-13 nm, while for the OA-coated nanoparticles it was 3-6 nm (TMO-I), respectively. These outcomes were in agreement with TGA results, according to which the nanoparticles synthesized under the same conditions, but with divergent carboxylic acids, contained significantly different amount of the organic phase. Determined from the TGA curves content of the stabilizer for the TMO-I (coated with OA) and TMY-V (coated with UA nanoparticles was of 20.6 % and 64.4%, respectively (Figure 9). Furthermore, considering the average particle diameter, densities of the particle core and organic shell, and content of the organic phase, the average thickness of the stabilizer layer was calculated, reaching the value of 1.4 nm for the TMO-I particles and 8.7 nm for the TMY-V ones. Base on the fact that length of OA molecule is of 1.9-2.1 nm, it can be assumed that the core of the TMO-I particle was coated with a monolayer of OA. In contrast, the shell thickness of

the TMY-V particles significantly exceeded the length of UA molecule (~1.7 nm), indicating the formation of a multilayer shell.

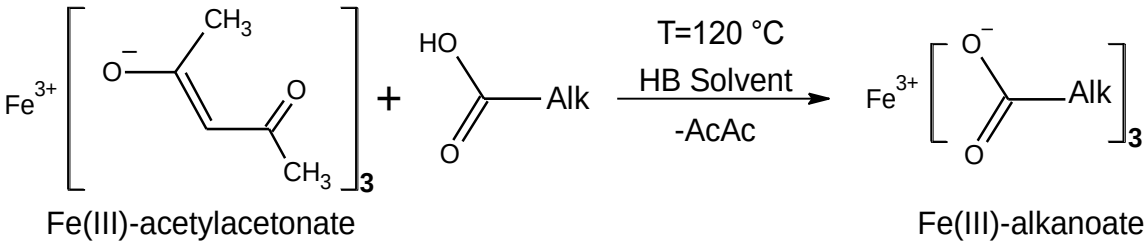

Figure 1: Formation of Fe(III)-alkanoate as a result of thermal decomposition of Fe(III)-acetylacetonate in the presence of higher carboxylic acid.

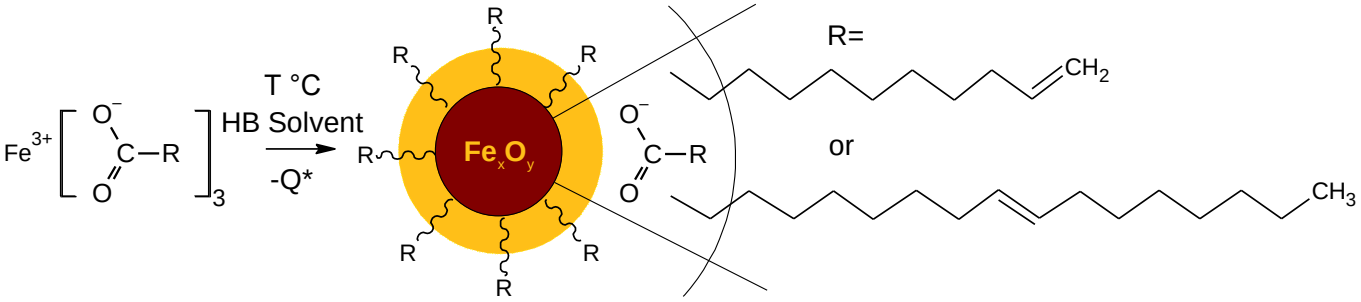

T=312 °C for octadecene; 255 °C for paraffin and bifenyl
Q*= H2, CO, CO2, higher ketone, hydrocarbons

Figure 2: Formation of nanoparticles via decarboxylation of Fe(III)-alkanoate.

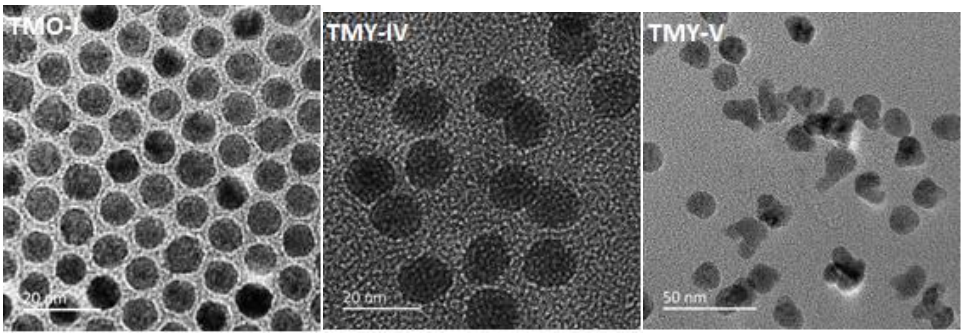

Figure 3: TEM micrographs of the nanoparticles synthesized in 1-octadecene using different stabilizers (TMO-I – OA, TMY-IV, TMY-V – UA).

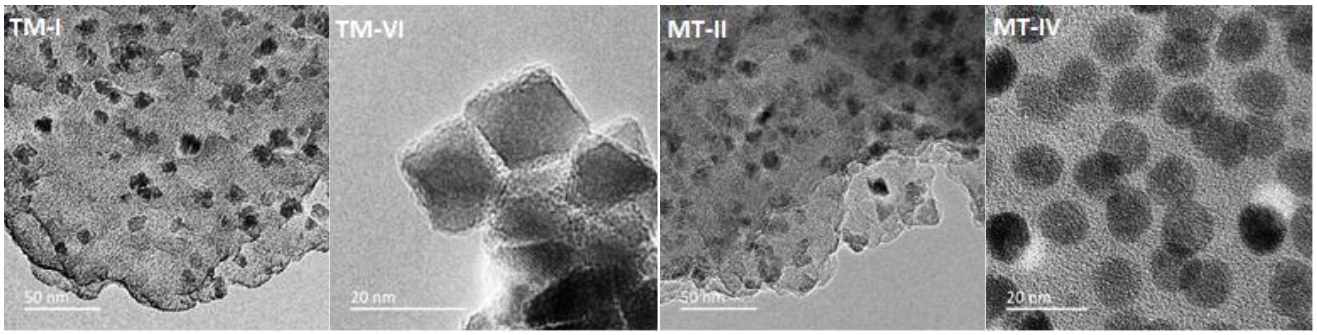

Figure 4: TEM micrographs of the nanoparticles synthesized using OA in paraffin (MT-II, MT-IV, MT-VI) and diphenyl (TM-I) in different conditions.

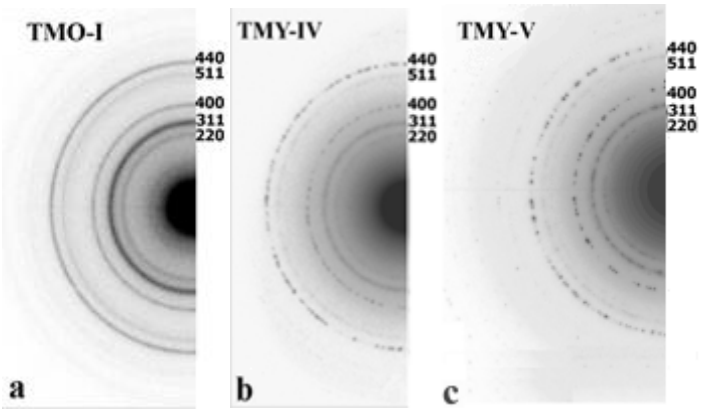

Figure. 5 Electron diffraction patterns of (a) TMO-I, (b)TMY-IV, (c) TMY-V.

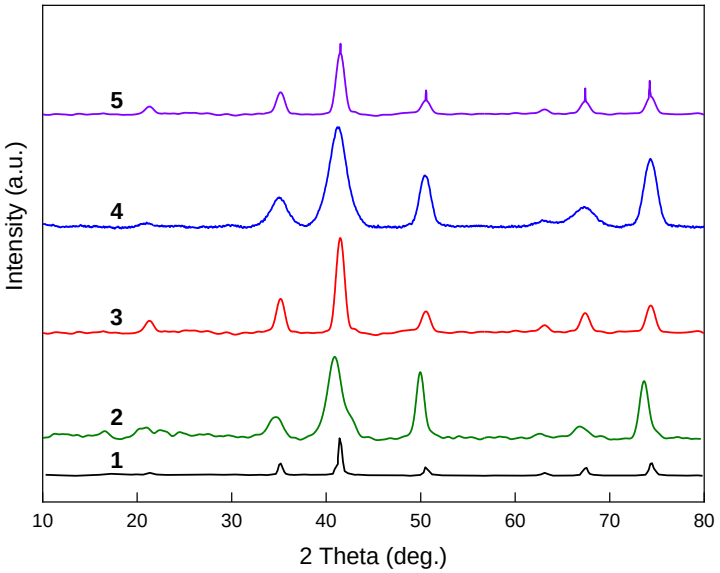

Figure 6: X-ray diffraction patterns of (1) Fe_3O_4 standard (JCPDS No. 88-315; mean crystallites size of 11 nm)[1], (2) TMY-V, (3) TM-VI , (4) TMO-I, and (5) γ-Fe_2O_3 standard (JCPDS No.00-039-1346)[28,29] .

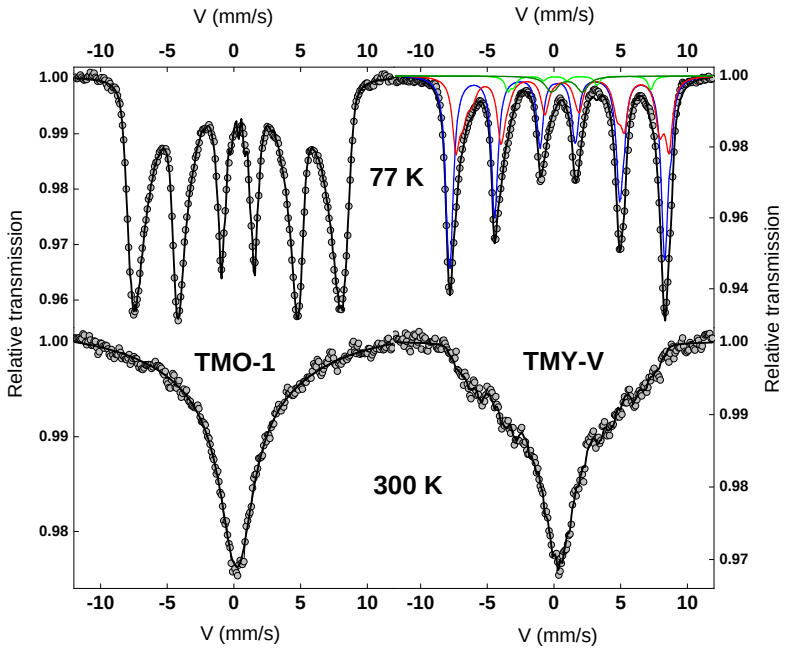

Figure 7: Mössbauer spectra of the TMO-I and TMY-V at 300 K and 77 K (blue, red, green and olive green correspond to Fe^{3+}, intermediate Fe^{3+}-Fe^{2+}, Fe^{2+} magnetic components and quadrupolar Fe^{2+} component, respectively).

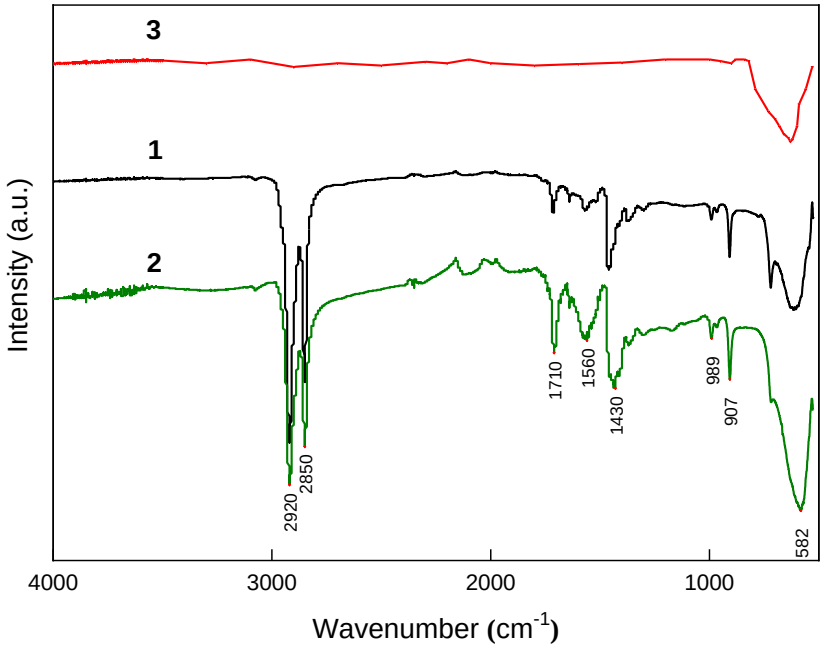

Figure 8: ATR FTIR spectra of the magnetic nanoparticles stabilized with 1) OA (TMO-I), 2) UA (TMY-II), 3) iron oxide powder without stabilizer (TM-III).

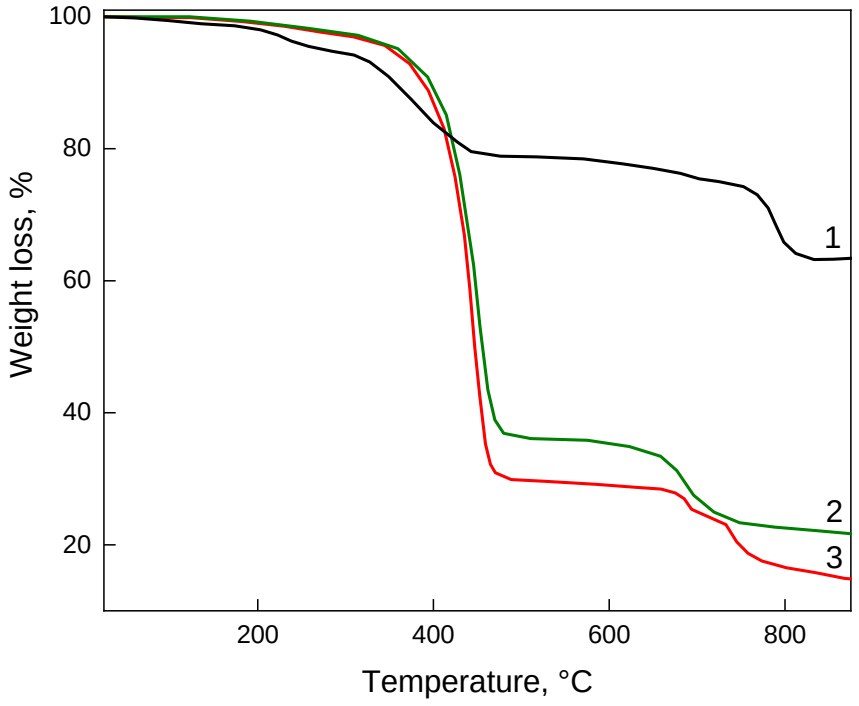

Figure 9: Thermogravimetric analysis of (1) TMO-I, (2) TMY-V and (3) TMY-IV .

Table 1: Synthesis conditions and characteristics of the obtained magnetic nanoparticles.

Sample name	Stabilizer	Fe(III)- acetylacetonate to carboxylic acid ratio (mol/mol)	Solvent	T (°C)	Stable dispersion	Size, D (nm)			I_{PCR} ×××	Polydispersity index, PDI
						TEM	DLS	XRD××		
MT-I	OA	1:3.29	diphenyl	255	±	7.5-12.5	*	8.8	1.7	
MT-II		1:3.37	paraffin		+	12**	*	*		
TM-III		1:3.05			-	-	-	-		-
MT-IV		1:3.30***			+	13	26	5.5	2,5	0.149
TM-VI		1:3.29			±	17*	*	8.8		-
TMO-I		1:3.30			+	8	14	4.6 (6.0×)	1.7 (1.3 ×)	0.089
TMO-III		1:5.60			-	-	-	-		-
TMY-II	UA	1:3.50	1-octadecene	310	+	13	34	6.9		0.242
TMY-III		1:5.80			-	-	-	-	-	-
TMY-IV		1:5.11			+	11	27	4.5	3.8	0.138
TMY-V		1:3.32			+	16	42	5.6	2.3	0.121

* – a significant number of units does not allow the analysis;
** – irregular nonspherical particles;
*** – two-fold lower concentration of the reagents;
× – with Rietveld refinement;
×× – according to Scherrer's formula [30];
××× – the polycrystallinity index calculated by the formula $I_{PCR} = D_{TEM} / D_{XRD}$ [31].

Conclusion

High-temperature decomposition of Fe(III)-acetylacetonate in the presence of exclusively higher unsaturated carboxylic acid (OA or UA), without additional co-stabilizers or reducing agents, on the principle of single-reactor synthesis, which involved the stage of formation of Fe(III)-alkanoates could be used to obtain monodisperse nanoparticles of iron oxide (Fe_3O_4, Fe_2O_3 or their mixtures) with controlled dimensions.

Different techniques, including X-ray diffraction and Mössbauer spectrometry, were used to investigate nanoparticles nature, and the presence of magnetite was found in bigger nanoparticles, showing that an oxidation phenomenon induced the formation of maghemite on the surface.

Experimental

Materials and methods

Fe(III)-acetylacetonate (Fe(III)-2,4-pentadienoate, 97%), undecylenic acid (UA; 96%), paraffin (used after recrystallization), diphenyl (99%), 1-octadecene (91%), propanone were purchased from Merck KGaA (Darmstadt, Germany). Oleic acid (OA; 98%) was bought from Lachema (Brno, Czech Republic). For magnetic separation, a permanent cylindrical neodymium magnet (NdFeB; 45x15 mm), with an induction on the surface of 1.2 T, was used. To characterize the size, morphology, hydrodynamic diameter, X-ray diffraction (XRD) and transmission electron microscopy (TEM), and dynamic light scattering (DLS, Malvern Zetasizer Nano S, Palaiseau, France) were used. TEM microscopic observations were conducted using a JEOL JEM 2100 HR microscopw (Croissy sur Seine, Francce) equipped with a LaB_6 source. An accelerating voltage of 200 kV was applied. The electronic diffraction patterns were obtained using selected area electron diffraction (SAED) technique. XRD diffraction patterns were collected using Panalytical MPD-PRO diffractometer equipped with a linear X'celerator detector

and Co Kα lamp as a source of radiation (1.789Å). The experimental data was analysed using HighScorePlus software, with implemented Rietveld method[32]. This method gives different types of crystallographic information such as size of the unit cell, the coordinates of the atoms, and the agreement indices that reflect a good refinement. The collected XRD patterns were compared with the standard of maghemite and magnetite available within International Centre for Diffraction Database (ICDD).

Certain structural and magnetic properties of the synthesized magnetic nanoparticles were studied by means of ^{57}Fe Mössbauer spectrometry at 77 K. The samples were investigated using a transmission conventional device with a Co source diffused into a Rh matrix. The hyperfine parameters were refined by using quadrupolar doublets and magnetic sextets with lorentzian lines. The values of isomer shift are quoted to that of α-Fe at room temperature (RT). Indeed, this technique is highly sensitive to the valency state of Fe species, and thus makes it possible to discriminate the presence of magnetite from that of maghemite and to estimate their respective proportions. Measurements were performed in transmission geometry with a 925 MBq γ-source of ^{57}Co/Rh mounted using a conventional constant acceleration drive. The velocity of the source was calibrated using α-Fe as the standard at RT. Measurement was performed on solid pellets made of dried nanoparticles containing about 5 mg Fe/cm^2. The Mössbauer spectra were fitted using the MOSFIT program (the Modular Open Source Fitter for Transients, a Python 2.7/3.x package for fitting, sharing, and estimating the parameters of transients via user-contributed transient models) involving quadrupolar and magnetic components with Lorentzian lines. The isomer shift values are referred to as that of α-Fe at RT.

ATR-FTIR measurement were performed on a ThermoScientifis iD5 ATR Nicolet iS5 IR spectrometer (Waltham, MA USA) on a diamond crystal. Thermogravimetric measurements were carried out using TA Instrument, Hi-Res-Dynamic TGA Q 500 (New Castle, USA) in a nitrogen atmosphere and the temperature range from 25 °C to 900 ºC (heating rate of 10

°C/min, N_2 flux 80 mL/min). Prior to the TGA measurements, nanoparticles were dried under vacuum at 50 °C prior to the TGA experiment.

Synthesis of iron oxide nanoparticles

The synthesis of nanoparticles was carried out in a 100 mL three-necked glass reactor equipped with a reflux condenser and mechanical stirrer. A Wood's metal alloy bath with temperature control within 100-400 °C was used for heating. Fe(III)-acetylacetonate (3 g, 8.49 mmol) was dissolved in a solvent (30 mL; diphenyl, 1-octadecene, or paraffin). Different molar ratios of carboxylic acid (OA or UA) to Fe(III)-acetylacetonate (in the ratio from 1:3.05 to 1:5.8) were used. The solution was heated up to 120 °C, and the acetylacetone (AcAc) was removed under a vacuum of 150 mm Hg with constant stirring. Then, the reflux condenser was replaced by an air condenser and the reaction mixture was heated up to the 255 °C in case of diphenyl and paraffin and 312°C under argon in case of 1-octadecene. The stirring was continued for 30 min. The resulting reaction mass was transferred into the 250 mL reactor equipped with a mechanical stirrer and washed five times with propanone (150 mL each time) nanoparticle deposition by magnetic separation on a NdFeB magnet. The supernatant was eliminated by decantation and the precipitate was suspended in 5 mL of hexane using ultrasonic bath UM-2, 140 W (Olsztyn, Poland). Hexane fractions were evaporated in a vacuum, and the remaining nanoparticles were resuspended in toluene to obtain a stable colloidal solution, which was stored under argon.

Acknowledgements

The work was performed with grant support within Ukraine (Projects M73-2019, M63-2020) - France (Project N°42580YF) R&D project of the programme PHC DNIPRO 2019.

Dr. Małgorzata Świętek (Institute of macromolecular chemistry CAS, Prague, Czech Republic) is gratefully acknowledged for language revision of the manuscript and valuable editorial comments.

References

1. Sandler, S.; Fellows, B.; Mefford, O. *Anal. Chem.;* **2019**, 91, 14159–14169. https://doi.org/10.1021/acs.analchem.9b03518.
2. Oleksa, V.; Macková, H.; Patsula, V.; Dydowitzová, A.; Janoušková, O.; Horák, D. *ChemplusChem*. **2020**, 85,1156-1163. https://doi.org/10.1002/cplu.202000360.
3. Wallyn, J.; Anton, N.; Vandamme, T. *Pharmaceutics* **2019**, 11, 601. https://doi.org/10.3390/pharmaceutics11110601.
4. Dandan, L.; Yingcai, H.; Yaping, L.; Chong, H.; Tak-Chun, Y.; Wai-Kin, Y.; Yu, Z.; Chi-Chun, F.; Weimao, W.; Siu-Kie, A.; Shubin, W.; Mengsu, Y. *Theranostics* **2020**, 10,1181–1196. . https://doi.org/10.7150/thno.38989.
5. Hergt, R.; Dutz, S.; Muller, R.; Zeisberger, M *J. of Physics: Condensed Matter.* **2006**, 18, 2919-2934. https://doi.org/10.1088/0953-8984/18/38/S26.
6. Świętek, M.; Brož, A.; Tarasiuk, J.; Wroński, S.; Tokarz, W.; Kozieł, A.; Błażewicz, M.; Bačáková, L. *Mater. Sci. Eng. C.* **2019**, 104, 109913. https://doi.org/10.1016/j.msec.2019.109913.
7. Park, E.; Umh, Y.; Choi, D.; Cho, M.; Choi, W.; Kim, S.; Kim, Y.; Kim, J. *Arch. Toxicol.* **2014**, 88, 1607-1618. https://doi.org/10.1007/s00204-014-1210-1.
8. Shixiang, L.; Bing, Y.; Song, W.; Youqing, S.; Hailin, C. *Adv. Coll Inter. Sci.* **2020**, 281,102165. https://doi.org/10.1016/j.cis.2020.102165.
9. Bedanta, S.; Kleemann, W. *J. Phys. D: Appl. Phys*. **2009**, 42,013001. https://doi.org/10.1088/0022-3727/42/1/013001.
10. Ghazanfari, M.; Kashefi, M.; Shams, S.; Jaafari, M. *Biochem. Res. Int*. **2016**, 2016, 7840161. https://doi.org/10.1155/2016/7840161.
11. Sen, T.; Shepard, S.; Mercer, T.; Eizadi-sharifabad, M.; Mahmoudi, M.; Elhissi, A. *RSC Advances* **2012**, 2, 5221-5228. https://doi.org/10.1039/C2RA20199B.
12. Sun, S.; Murray, C.; Weller, D.; Folks, L.; Moser, A. *Science*, **2000**, 287, 1989-9192. https://doi.org/10.1126/science.287.5460.1989.
13. Sun, S.; Zeng, H. *J. Am. Chem. Soc*. **2002**, 124, 8204-8205. https://doi.org/10.1021/ja026501x.
14. Sun, S.; Zeng, H. *J. Am. Chem. Soc.* **2004**,126, 273-279. https://doi.org/10.1021/ja0380852.
15. Gul, S.; Khan, S.; Rehman, I.; Khan, M.; Khan, M. *Front. Mater.* **2019**, 6, 1-15. https://doi.org/10.3389/fmats.2019.00179.
16. Khurshid, H.; Li, W.; Chandra, S.; Phan, M.; Hadjipanayis, G.; Mukherjee, P.; Srikanth, H. *Nanoscale* **2013**, 5, 7942. https://doi.org/10.1039/C3NR02596A.
17. Hou, Y.; Xu, Z.; Sun, S. *Angew. Chem.; Int. Ed.;* **2007**, 46, 6329 —6332. https://doi.org/10.1002/ange.200701694
18. Li, X.; Si, H.; Niu, J.; Shen, H.; Zhou, C.; Yuan, H.; Wang, H.; Ma, L.; Li, L. *Dalton Trans* **2010**, 39, 10984-10989. https://doi.org/10.1039/C0DT00965B.
19. Patsula, V.; Petrovský, E.; Kovarova, J.; Konefał, R.; Horák, D. *Colloid Polym. Sci.* **2014**, 292, 2097-2110. https://doi.org/10.1007/s00396-014-3236-6.
20 Bruce, I.; Taylor, J.; Todd, M.; Davies, M.; Borioni, E.; Sangregorio, C.; Sen, T. *J. Magn. Magn. Mater*. **2004**, 284,145-160. https://doi.org/10.1016/j.jmmm.2004.06.032.
21. Roca, A.; Morales, M.; Serna, C. *IEEE Trans. Magn*. **2006**, 42, 3025-3029. https://doi.org/10.1109/TMAG.2006.880111.
22. Ronald, A.; Biemann, K. *J. Am. Chem. Soc.*; **1972**, 94, 5772-5777. https://doi.org/10.1021/ja00771a039.
23. Bronstein, L.; Huang, X.; Retrum, J.; Schmucker, A.; Pink, M.; Stein, B.; Dragnea, B. *Chem. Mater.* **2007**, 19, 3624-3632. https://doi.org/10.1021/cm062948j.

24. Liu, K.; Zhao, L.; Klavins, P.; Osterloh, F.; Hiramatsu, H. *J. Appl. Phys.* **2003**, 93, 7951-7953. https://doi.org/10.1063/1.1556133.
25. Demortiere, A.; Panissod, P.; Pichon, B.; Pourroy, G.; Guillon, D.; Donnio, B.; Begin-Colin, S. *Nanoscale*, **2011**, 3, 225-232. https://doi.org/10.1039/c0nr00521e.
26. Park, J.; An, K.; Hwang, Y.; Park, J.; Hon, H.; Kim, J.; Park, J.; Hwang, N.; Hyeon, T. *Nat. Mater.* **2004**, 3, 891-895. https://doi.org/10.1038/nmat1251.
27. Dehant, I.; Danz, R.; Kimmer, V.; Schmolke, R. *Infrared Spectroscopy of high-polymers*, Moscow,1976.
28. Kurapov, Y.; Vazhnichaya, E.; Litvin, S. *Applied Sciences.* **2019**, 1, 102. https://doi.org/10.1007/s42452-018-0110-z.
29. Deeprasert, S.; Wang, L.; Simeonidis, K.; Thanh, N.; Duguet, E.; Mourdikoudis, S. *RSC*. **2021**, 11, 1343-1353. https://doi.org/10.1039/D0RA09907D
30. Cullity, B.; Stock, S. *Elements of X-Ray Diffraction,* 3rd Edition, Pearson Education Limited, 2014. ISBN-13: 978-0201610918, ISBN-10: 0201610914.
31. Theivasanthi, T.; Alagar, M., *Nano. Biomed. Eng.* **2012**, 4, 58-65. https://doi.org/10.5101/nbe.v4i2.p58-65.
32. Albinati, A.; Willis, B. *J. Appl. Cryst.* **1982**, 15, 361-374. https://doi.org/10.1107/S0021889882012187.